Global real-time detection of major floods using passive microwave remote sensing

T. De Groeve [a,*], P. Riva [a]

[a] Joint Research Centre of the European Commission, Via Fermi 2147, 21020 Ispra, Italy – tom.de-groeve@jrc.it

Abstract – **Space-based river monitoring can provide a systematic, timely and impartial way to detect floods of humanitarian concern. This paper presents a new processing method for such data, resulting in daily flood magnitude time series for any arbitrary observation point on Earth, with lag times as short as 4h. This results in a daily update of major floods in the world, with an objective measure for their magnitude, useful for early humanitarian response. The technique is demonstrated on the 2009 floods in Southern Africa.**

Keywords: Global flood detection, microwave remote sensing.

1. INTRODUCTION

Although floods are the most frequent and recurring natural disasters (46%) consuming up to one third of humanitarian aid (FTS OCHA, 2009) and affected 78% of all people affected by natural disasters (OFDA/CRED, 2006), there is no systematic, global and timely monitoring system available yet.

Floods are difficult to monitor, because they are determined by local factors such as precipitation, slope of the terrain, drainage of the river, protection devices in place, etc. Each river must be monitored at different places along its course. Although some flood disasters occur annually, most happen unexpectedly. The 2641 floods disasters recorded in the Dartmouth Flood Observatory catalogue (DFO, 2009), one of the most complete archives of flood events, between 2000 and 2007 affected 2051 different rivers. Some rivers flooded more than 10 times (at different places along their course), but 1133 rivers flooded only once in 7 years. All rivers must therefore be monitored, and along their full course. The number of rivers in the world is hard to determine, but even VMAP0, a database at scale 1:1 million which shows only major rivers, has close to 1 million records, with a total length of 10 million km. In situ global flood monitoring system would need a dense network of gauging stations along all rivers. However, such stations are expensive (the United States Streamgaging Network costs 89 million US$ per year; USGS, 1998), which makes this hardly feasible on a global scale.

1.1 Satellite based flood monitoring

Alternatively, in situ measurements can be replaced by remote sensing measurements, from airplanes or satellites. The change in surface water extent can be extracted from aerial or satellite imagery. While the use of sensors in the visible or infrared portion of the spectrum is limited due to cloud cover, the microwave portion of the spectrum can penetrate clouds (Smith, 1997). However, for most remote sensing solutions, the revisit frequency (i.e. the time between two measurements in the same place) is too low for monitoring purposes or the spatial coverage is limited

(Bjerklie et al., 2003). For satellite based imagery, the revisit time depends on the orbit and the image size, and at least a few sensors have daily revisit time, global coverage and provide microwave data in near-real time free of charge. These are the Advanced Microwave Scanning Radiometer - Earth Observing System (AMSR-E) instrument on board of the NASA EOS Aqua satellite (launched in 2002) and the Tropical Rainfall Monitoring Mission (TRMM).

Using AMSR-E data, De Groeve et al. (2006) developed a method for detecting major floods on a global basis in a systematic, timely and impartial way appropriate for humanitarian response. Brakenridge et al (2005) demonstrated that AMSR-E can measure river discharge changes in various climatic conditions. The methodology uses the brightness temperature at 36.5GHz H-polarization during the descending (night) orbit of AMSR-E with a footprint size of approximately 8x12km2 and an average revisit time at 1 day. Brightness temperature is related to the physical temperature T and the emissivity ε of an object: $T_b = \varepsilon.T$. Due to the different thermal inertia and emission properties of land and water the observed microwave radiation in general accounts for a lower brightness temperature values for water ($T_{b,water}$) and higher for land ($T_{b,land} > T_{b,water}$). Since the each observation of the satellite (or pixel) covers a relatively large area of 8x12km2, the observed brightness temperature is mostly composed of both water and land values, in proportion to the relative area of water (w) and land ($1 - w$) in the pixel.

$$T_b = (1-w)T_{b,land} + wT_{b,water} \qquad (1)$$
$$w = \text{water portion of the pixel}$$

If the physical temperature remains constant, changes in brightness temperature will be related to changes in water surface extent in the pixel. However, in spite of the great radiation dissimilarity of water and land cover, the raw brightness temperature observations cannot be used to reliably detect changes in surface water area. This is because brightness temperature (T_b) measures are influenced by other factors such as physical temperature, differences in emissivity and atmospheric moisture. While the relative contribution of these factors cannot be measured, the authors assume them to be constant over a larger area. As shown in equation 2, the ratio between two nearby pixel values is a function of w alone. Therefore, by comparing a "wet pixel" received over a river channel of a potential inundation location ($w > 0$) with a "dry pixel" without water cover ($w = 0$) the mentioned noise factors can be reduced. The brightness temperature values of the measurement/wet signal are divided by the calibration/dry observations, referred to as M/C ratio or signal s.

$$T_{b,measurement} = (1-w)T_{b,land} + wT_{b,water}$$
$$= T_{measurement}\left((1-w)\varepsilon_{land} + w\varepsilon_{water}\right) \quad (2)$$
$$T_{b,calibration} = T_{b,land} = T_{calibration}\varepsilon_{land}$$

If for nearby pixels we assume

$$\varepsilon_{land,measurement} \approx \varepsilon_{land,calibration} \approx \varepsilon_{land}, T_{measurement} \approx T_{calibration} \quad (3)$$

then

$$s = \frac{M}{C} = \frac{T_{b,measurement}}{T_{b,calibration}} = \frac{T_{measurement}\left((1-w)\varepsilon_{land} + w\varepsilon_{water}\right)}{T_{calibration}\varepsilon_{land}}$$
$$\approx 1 - w + w\frac{\varepsilon_{water}}{\varepsilon_{land}} = f(w) \quad (4)$$

Typically, emissivity values of water are around 0.5 and of most minerals between 0.75 and 0.95 (Rees, 1990). When calibration pixels are chosen carefully (without any open water), *s* varies between 1 ($w = 0$, no water) and 0.3 to 0.5 ($w = 1$, fully flooded) depending on the mineral content of the soil. In a time series, *s* is expected to vary with changes in water surface. Anomalies of the signal *s* can be correlated well with flood events. Moreover, as demonstrated by Brakenridge *et al.* (2007), if gauging data is available for the site, the signal can be calibrated to staging height with accurate results.
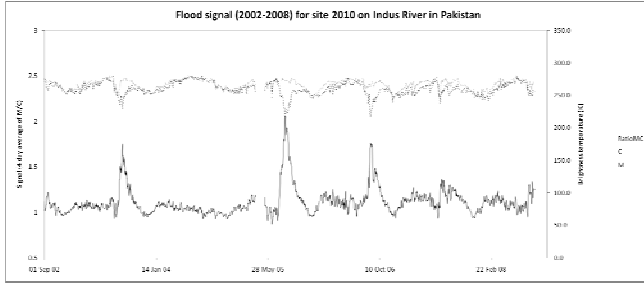

Figure 1. Example of time series of $T_{b,measurement}$ (*M*), $T_{b,calibration}$ (*C*) and the flood signal *s* (*RatioMC*) for site 2010 100km north of Hyderabad on the Indus River in Pakistan. The three peaks correspond to true flood disasters in 2003, 2005 and 2006 (from De Groeve *et al.*, 2009).

De Groeve and Riva (2009) showed that a local maximum in a moving window can be used for the calibration value, avoiding the need for manual selection of the calibration site. This finding makes the method applicable in any arbitrary area on Earth, rather than in carefully chosen sites, opening the way for a global flood detection system.

This paper describes a methodology to detect floods based on the method described before.

2. DATA

The methodology has been tested with AMSR-E data and TRMM data. However, TRMM data is only available up to latitudes of 30 degrees. In order to have global coverage, AMSR-E data is used.

The data used is the Level 1 brightness temperature at 36.5GHz H-polarization during the descending (night) orbit of AMSR-E with a footprint size of approximately 8x12km2 and an average revisit time of 2 days south of 30 degrees and 1 day north of 30 degrees latitude. The swath data is available about 4h after acquisition by the satellite from the Japanese Space Agency (Jaxa).

The data is downloaded at JRC, resampled (using a nearest neighbor approach) and mosaicked in daily grids with global coverage (see De Groeve and Riva, 2009 for a detailed description of the data processing steps). The result is global grid (4000 by 2000 pixels) of brightness temperature data, available by date. The data of the current day is recalculated whenever new swath data is available.

Flood signals are calculated as soon as new data is available. Using the local 95 percentile in a window of 7x7 pixels as the calibration temperature, the signal (M/C value) is calculated for each pixel, resulting in a "signal image".

3. METHODS

In order to distinguish between areas with permanent water (e.g. lakes or wide rivers) and areas with flood waters, we look at change in flood signal over time. Based on a time series of 7 years (going back to June 2002 when the satellite was launched), anomalies are automatically detected using a method described in De Groeve *et al.* (2006). Since lower M/C signals generally accounts for increased water coverage, extreme events, or major floods, should represent negative anomalies in the time series of a given site. In order to detect anomalies, they first determined the reference value for normal flow, which varies for each site based on the local emissivity properties and river geometry. This reference value was calculated as the average M/C value for the site since the launch of the satellite. They then set flood level thresholds based on the statistics of the time series. Flood magnitude was defined as the number of standard deviations (sd) from the mean (avg):

$$m = \frac{s - avg(s)}{sd(s)} \quad (3)$$

Floods appear typically for anomalies of 2 (small and regular flood) or 4 (large and unusual flood). This is equivalent to probabilities of 2.1% and 0.003%.

With the signal images, a similar method can be applied. However, because no calibration site is necessary, the magnitude can be calculated for any arbitrary point or area. To observe an area, we define an observation area as a collection of pixels. For these observation areas, a set of quantities are calculated including: average magnitude, maximum magnitude, number (an percentage) of pixels exceeding magnitude 2 and number (and percentage) of pixels exceeding magnitude 4.

All these quantities are indicative of the size of the flood in the observation area. The average or maximum magnitude is an objective measure of the degree of flooding, while the pixel count is a measure of the extent of the floods. Since each pixel represents an area of 100km2, the "number of pixels exceeding magnitude 4" are an approximate measurement of the flooded area (number of pixels x 100km2).

4. RESULTS

The result of the method was tested during the recent floods in Southern Africa. At the end of February, severe flooding started in along the Upper Zambezi and in the Northern areas of Namibia in the aftermath of persistent and severe rainfall. In particular people in the area of Caprivi were affected. At least 200000 people are affected and crops are washed away. For the floods in Northern Namibia and Southern Angola, the Namibian government declared a state of emergency. The floods have reportedly killed 90 persons and displaced up to 20000.

Three areas were analyzed with the method described in this paper (see Figure 2). For all areas, the time series of the average magnitudes were calculated, and the number of pixels exceeding magnitude 2 and 4 were counted over time.

Figure 2. Test areas: floods in Southern Africa, Spring 2009. Animation available at http://www.gdacs.org/floods.

In the border are of Namibia and Angola, Figure 3 shows the average magnitude and the percentage of pixels with magnitude over 4. Average magnitude peaks on 4 March 2009. But as early as 15 February, the flooded area sharply increases, indicating the start of the floods, although they were reported only later (the Dartmouth Flood Observatory mentions a starting date of 1 March). The peak of the flood was reached on 4 March 2009, when not only the Etosha Pan (in the South of the observation area) was flooded, but also the marshy area closer to the border. The town of Odjiva, Angola, is also in the flooded area. At the peak, around 25% of the observation area was flooded (with magnitude > 4), equivalent to 21200km^2.
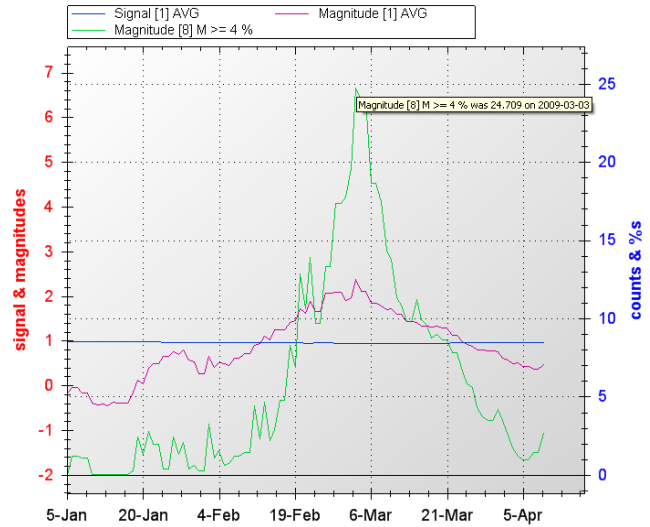

Figure 3. Time series of flood magnitude (purple) and percentage of area flooded (green). At the peak on 4 March 2009, around 25% of the area was flooded (magnitude > 4), equivalent to 21200km^2.

In the Caprivi Region, there is a clear rising in magnitude starting around mid-February. Around 20 March, there is a sharp increase in number of pixels with magnitude over 4, indicating the beginning of the floods. The floods peaked on 26 March, when 1900km^2 were flooded. The area of the flood is confirmed by maps based on optical image at medium resolution (250m) (e.g. as created by DFO and UNOSAT). The temporal aspect of flood measurements is important to provide a historical perspective. For instance, measurements show that the Caprivi floods are the worst since recording began in 2002. The floods in 2003 and 2004 are 60% and 80% respectively in size of this year's floods.
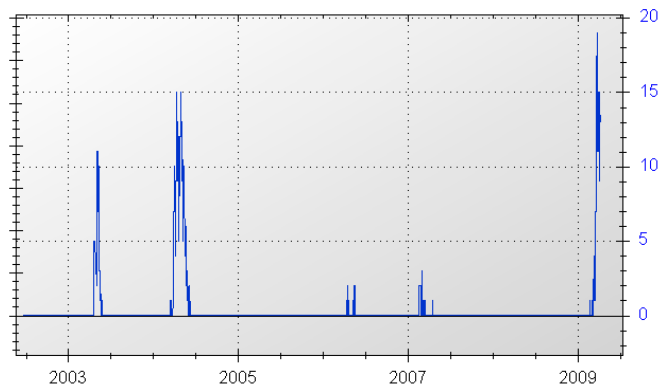

Figure 4. Time series for flooded area (number of pixels with magnitude > 4). The maximum is 1900km^2, compared to 1500km^2 in 2004 and 1100km^2 in 2003.

Anecdotal evidence gathered by the Dartmouth Flood Observatory from media reports confirm the starting date of the 2004 flood stating "April 1 - Zambezi river burst banks along eastern border of Caprivi strip, Namibia". Our system measured a sharp increase in flood coverage (up to 1500km^2 with very unusual flooding) on April 1st, coinciding with reports on river burst and high water.
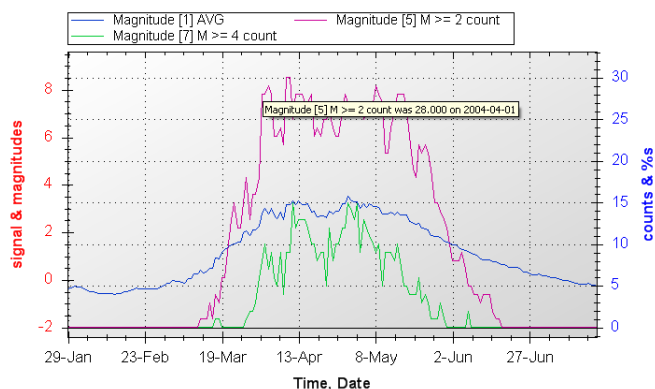
Figure 5. Detailed GFDS measurements for 2004 floods. The maximum values are reached around April 1st, consistent with DFO reports on river burst.

5. DISCUSSION

Many case studies including the ones described in this paper show that the system is able to provide precise data on starting and ending dates of floods and the size of the floods. While the absolute values of the flood size has not been validated sufficiently against alternative data sources, the relative values are consistent with anecdotal evidence. For instance, for the case studies in this paper, we calculated the average flooded area during 4 months (from February to May, Table 1). It is clear that the 2009 floods are worse the previous years, even if the flood season is still ongoing.

Table 1. Average flooded area (km^2) from February to May (4 months) of each year.

	Border Namibia Angola	Caprivi Region	Upper Zambezi
2009	2000	1330	1330
2008	1360	700	260
2007	300	60	190
2006	280	160	90
2005	80	140	30
2004	60	180	610
2003	120	15	450

6. CONCLUSIONS

This paper shows the accurate flood monitoring results obtained with passive microwave remote sensing, both in terms of flood extent and flood start and duration. Extent measurements are validated by comparing with optical high resolution satellite imagery. Start time and duration are validated with the Dartmouth Flood Observatory catalogue and media sources. Applied to the recent floods in Southern Africa, the technique allows to have a quantitative assessment of the size of the floods, either relative to previous years or in absolute terms.

7. REFERENCES

Bjerklie, D. M., S. Lawrence Dingman, Charles J. Vorosmarty, Carl H. Bolster, Russell G. Congalton (2003) Evaluating the potential for measuring river discharge from space, Journal of Hydrology, Volume 278, Issues 1-4, 25 July 2003, Pages 17-38, ISSN 0022-1694, DOI: 10.1016/S0022-1694(03)00129-X.

Brakenridge, G. R., Nghiem, S. V., Anderson, E., Chien, S. (2005) Space-based measurement of river runoff. Eos 86 (19), pp. 185-188.

Brakenridge, G. R., S. V. Nghiem, E. Anderson, and R. Mic (2007) Orbital microwave measurement of river discharge and ice status, Water Resources Research, 43, W04405.

De Groeve T., Z. Kugler, G. R. Brakenridge (2006) Near Real Time Flood Alerting for the Global Disaster Alert and Coordination System, Proceedings ISCRAM2007 (B. Van de Walle, P. Burghardt and C. Nieuwenhuis, eds.), pp. 33-39.

De Groeve, T., A. Annunziato, Z. Kugler and L. Vernaccini (2009) Near real-time global disaster impact analysis, in Information Systems for Emergency Management, Edited by Bartel Van de Walle, Murray Turoff, and Starr Roxanne Hiltz, in press.

De Groeve, T. and P. Riva (2009) Early flood detection and mapping for humanitarian response. Proceedings of the 6th International ISCRAM Conference – Gothenburg, Sweden, May 2009, J. Landgren, U. Nulden and B. Van de Walle, eds. [in press].

DFO, 2009. Dartmouth Flood Observatory Global Active Archive of Large Flood Events, http://www.dartmouth.edu/~floods (last accessed 25 February 2009).

FTS OCHA, 2009. Financial Tracking Service of the Office for Coordination of Humanitarian Affairs, http://ocha.unog.ch/fts (last accessed 25 February 2009).

GRDC, 2009. Tabular Summary and Statistics of GRDC stations, alphabetically sorted by countries. grdc.bafg.de (last accessed 25 February 2009).

Kugler Z. and T. De Groeve (2007) The Global Flood Detection System. EUR 23303 EN, Luxembourg: Office for Official Publications of the European Communities, 45p.

OFDA/CRED (2006) 2005 disasters in numbers, OFDA/CRED, http://www.em-dat.net (last accessed 11/01/2009).

Rees, 1990. Physical Principles of Remote Sensing. Cambridge, Cambridge University Press, 1990, 237pp.

Smith, L. C., 1997. Satellite remote sensing of river inundation area, stage, and discharge: A review. Hydrol. Processes 11, 1427-1439.

USGS, 1998. A New Evaluation of the USGS Streamgaging Network. A report to Congress. http://water.usgs.gov/streamgaging/report.pdf (last accessed 25 February 2009).